Impact of static and dynamic load models on security margin estimation methods

Hannes Hagmar [*],[a], Le Anh Tuan [a], Robert Eriksson [b]

[a] *Chalmers University of Technology, Department of Electrical Engineering, Gothenburg 412 96, Sweden*
[b] *Svenska kraftnät (Swedish National Grid), Sundbyberg 172 24, Sweden*

ARTICLE INFO

ABSTRACT

The post-contingency loadability limit (PCLL) and the secure operating limit (SOL) are the two main approaches used when computing the security margins of an electric power system. While the SOL is significantly more computationally demanding than the PCLL, it can account for the dynamic response after a disturbance and generally provides a better measure of the security margin. In this study, the difference between these two methods is compared and analyzed for a range of different contingency and load model scenarios. A methodology to allow a fair comparison between the two security margins is developed and tested on a modified version of the Nordic32 test system. The study shows that the SOL can differ significantly from the PCLL, especially when the system has a high penetration of loads with constant power characteristics or a large share of induction motor loads with fast load restoration. The difference between the methods is also tested for different contingencies, where longer fault clearing times are shown to significantly increase the difference between the two margins.

1. Introduction

Electric power systems are generally operated according to the $N-1$ contingency criterion, meaning that the system should be able to withstand the loss of any single system component, such as a transmission line or a generating unit, without losing stability. A system capable of handling this is said to be *secure* [1]. However, even when the system is secure for a given operation condition, system operators are also required to know how far the system can move from its current operating point and still remain secure. Therefore, system operators continuously compute *security margins*, which in turn represents the available transmission capacity in the system.

Two main approaches are used to compute the security margins of a power system: the post-contingency loadability limit (PCLL) and the secure operating limit (SOL) [1,2]. The PCLL is evaluated by estimating the loadability limit of a post-contingency operating point, where a solution path is traced by iteratively increasing the system stress until the system's critical point is reached. The characteristics of the iteratively increased system stress in the post-contingency setting are similar to that of the slow load restoration that typically follows in a long-term voltage stability event. An alternative measure of the security margin is the SOL, which refers to the most stressed *pre-contingency* operating state in which

the system can withstand a specified set of contingencies. The SOL, also referred to as the dynamic security margin, can account for the dynamic response after a disturbance and it generally provides a more accurate measure of the security margin of the system. However, the SOL has been comparatively less documented in the literature, likely due to the practical difficulties required in its estimation. The SOL requires numerous full time-domain or quasi steady-state (QSS) simulations to trace the security limit for a set of different contingencies, a task that is generally too time-consuming to meet the near real-time monitoring requirements of system operators.

A security margin's capability to account for the dynamic response after a disturbance is likely to become increasingly important in the future. Electric power systems are experiencing a significant transformation; primarily characterized by increased penetration of power electronic converter interfaced technologies [3]. This type of components may have a significant influence on system stability, and includes the impact of dynamic load models [4], converter interfaced generation [5,6], high-voltage direct current (HVDC) systems [7], as well as battery energy storage devices and flexible ac transmission systems [8,9]. With the significant integration of such technologies, the dynamic response of power systems will in general become more dependent on fast-response devices, altering the power system dynamic behavior.

---

* Corresponding author.
E-mail address: hannes.hagmar@chalmers.se (H. Hagmar).

Although the SOL would provide a better measure of the security margin in a future with a higher share of fast-acting loads and generation, the high computational effort required in its estimation limits its possible applications. Several studies have attempted to provide solutions to the high computational effort required in estimating the SOL. Methods based on QSS simulations work by replacing the short-term differential equations of generators, motors, compensators with the corresponding algebraic equilibrium equations, thus significantly simplifying the general dynamic model of the power system [1]. Estimation methods for the SOL that are based on QSS simulations, as found in [10], can reduce the simulation time significantly compared to full time-domain simulations, but cannot fully incorporate the impact of short-term and transient effects. In [11], a method that combined QSS and time-domain simulations was proposed to include the impact of short-term effects. In [12], the authors used real synchrophasor data from the Hydro-Québec's transmission system to baseline phase-angles versus actual transfer limits across system interfaces. A method for forecasting the SOL was then developed using ensemble decision trees where medoid clustering of the phase shift data was used as predictive features. In [13–15], various machine learning approaches based on training neural networks were proposed to allow real-time estimation of the SOL, with a specific focus on voltage stability. In [16], a combined methodology based on validating the estimations of neural networks with actual time-domain simulations was proposed to overcome the robustness issues that are commonly related to machine learning methods.

Despite ongoing efforts in improving the computational efficiency of the SOL, the circumstances when the SOL is to prefer to the PCLL have been relatively unexplored in the literature. In [17], it was shown that if a system starts at a stable equilibrium and is slowly stressed towards a critical point without encountering oscillations or other limit-induced events (e.g. reactive power limits for generators), static estimation methods are sufficient to locate the exact critical point experienced by the dynamic system. Thus, in such circumstances, the security margin computed by PCLL would essentially be equal to the one computed using the method of the SOL. In [16], a theoretical comparison between the two security margins was performed with respect to voltage stability, where the difference between the two measures was illustrated using a concept called "transient *P-V* curves". The study highlighted the importance of load restoration dynamics on the difference between the two methods but provided no numerical results. In [18], the SOL was numerically compared to another type of security margin computed by static $V - Q$ curves, in which variations in the reactive power injection at a bus would affect the voltage at that same bus. The study concluded that the SOL (or generally a dynamic simulation approach) is a superior method compared to $V - Q$ curves, but since the two methods are so conceptually different, the results of the two methods could not directly be compared. In [10], the SOL computed by QSS simulations was compared to the PCLL, where primarily the impact of post-disturbance control was studied. No variations in the load composition were analyzed in the study.

A direct comparison between the SOL and PCLL is however not trivial, as one is computed using a static model of the system, while the other is generally estimated using a dynamic model. Thus, although it is well-known that the PCLL and the SOL may produce significantly different estimations of the security margin, the difference in the results can be caused by both in *how* the simulations were conducted, as well as owing to the fact that the SOL can account for the system's dynamic response after a disturbance. To address the above-mentioned lack of an accurate comparison between the methods, this study aims to develop a methodology that allows the two security margins to be fairly compared and to isolate the root cause of the difference between the two security margins. Further, we also provide a comparison for a large range of different static and dynamic load configurations and disturbance scenarios that are based on the developed methodology. We focus on the impact that different load model configurations and disturbances have

on the two defined security margins. It should be noted that other aspects, such as post-disturbance controls and generation characteristics of, for instance, converter-interfaced generation, will also have a significant impact on the difference between the two security margins and such studies deserves further attention in future research. The two security margin methods are analyzed mainly with respect to the following stability criteria: short-term and long-term voltage stability and rotor (transient) angle stability. The impact that frequency stability may have on the two security margins has not been analyzed in the study.

The main contributions of this study can be summarized as:

- A methodology to allow a fair comparison between the PCLL and the SOL is developed. The purpose of the developed methodology is to isolate the root cause of the difference between the two security margins; that is, that the PCLL is computed by the loadability limit of a *post-contingency* operating state, whereas the SOL is computed by the loadability limit to the final *pre-contingency* operating state in which the system is still secure. Any difference between the security margins caused by differences in the simulations and the simulation setups is compensated for.
- An extensive numerical comparison between the SOL and the PCLL under a range of both static and dynamic load model configurations is performed. Different fault scenarios are examined and discussed in the study. The purpose is to examine under what circumstances that the SOL is preferable to the PCLL. While the results are specific for the used test system, they are used to illustrate for which load and disturbance scenarios the difference between the PCLL and the SOL becomes most significant.

The rest of the paper is organized as follows. In Section 2, the security margin definitions for the SOL and the PCLL are presented. In Section 3, the methodology used in computing the margins is presented along with the simulation platform and the adaptations used to allow a fair comparison between the security margins. Results and discussion are presented in Section 4. Concluding remarks are presented in Section 5.

2. Security margin definitions

In this section, a theoretical comparison between the PCLL and the SOL is presented. The conceptual difference of computing the two security margins is first presented, which is followed by a theoretical analysis of the circumstances and the instability mechanisms that can cause the two methods to differ.

2.1. PCLL versus SOL

The security margin estimation processes for the PCLL and the SOL are illustrated in Fig. 1. Pre-contingency and post-contingency *P-V* curves are used where a receiving end voltage in a stressed area is a function of an increasing (active) power transfer from the system to this receiving end. An initial, unstressed, operating condition (OC) is the starting point for the security margin estimation. The security margin is then defined as the change in loading from the initial OC to the $N - 1$ critical point. It should be noted that in actual applications, the limit is often smaller due to the other stopping criteria such as too low system voltages. However, for better illustration purposes, the former limit is used here.

In PCLL estimation, a post-contingency operating point is found by first introducing a contingency on the initial OC, which is typically followed by solving the resulting power flow study. This is illustrated in Fig. 1 by moving along arrow I'. The security margin is then traced along the solution path by iteratively and step-wise increasing the system stress until the critical point is reached, moving along the arrow $2'$. Parameterized continuation methods based on static load flow solutions, generally referred to as continuation power flow (CPF), are commonly

used to avoid convergence problems close to the critical point of the system [19]. The distance between the pre-contingency operating point and the $N - 1$ critical point represents the PCLL.

In the estimation of the SOL, the dynamic security of the system is tested with an increasing stress level, illustrated by arrow *1* in Fig. 1 [10]. For every new stressed pre-contingency OC, the system response following the disturbance is studied. The final, pre-contingency OC that is tested and can provide a stable operating point is illustrated by moving along arrow *2* in Fig. 1. The state transition following arrow *2* can generally not be computed using static methods as it can result in numerical divergence. Instead, methods based on dynamic (or QSS) simulations are generally required. The increased loadability between the initial OC and the most stressed pre-contingency OC that can still handle a dimensioning contingency without causing instability represents the SOL. It should be noted, that while the PCLL and the SOL are illustrated to result in the same level of security margin in Fig. 1, this is generally *not* the case. The difference between the two security margins is further analyzed in the following sections and a typical case is exemplified in Fig. 2.

2.2. System dynamics and instability mechanisms

Loads are often recognized to maintain constant power characteristics in a long-term *system* perspective but do not generally behave as such following a disturbance. Assuming a sudden voltage change, loads will initially drop according to their instantaneous characteristics [20]. Then, the impedance or the drawn current is adjusted to restore the load to its original level; a process that can be exemplified by the automatic changes in the slip of induction motors or by changes in tap positions to increase the voltage for loads behind load tap changers (LTCs). The overall load restoration after a disturbance is generally assumed to act significantly slower than the dynamics of other system components, such as the dynamics of generators and excitation systems. The PCLL is based on this time-scale decomposition, where short-term dynamics, such as the slip of induction motors, or generator and excitation dynamics, are assumed to be in equilibrium. Using this assumption, the loadability limit of the post-disturbance system can be found even though only static estimation methods are used to trace the security margin.

In [20] and [16], the concept of *transient P-V* curves was used to allow visualization and analysis of short-term dynamics using *P-V* curves. In the analysis, the post-disturbance $P - V$ curve is not fixed in time but is allowed to be affected by short-term system dynamics of, for instance, excitation systems. Nor is the load curve fixed in time, which allows the load restoration that follows after a disturbance to be illustrated. In Fig. 2, transient *P-V* curves are used to illustrate a system that, when assuming the short-term dynamics are in equilibrium, could appear to be secure. However, when the short-term dynamics are taken into account, there is a loss of post-disturbance equilibrium of the short-term dynamics, and the disturbance would in fact cause the system to become unstable. The load restoration curves and the transient *P-V* curves are illustrated using different shades of grey, where a lighter shade indicates closer in time after the disturbance. The time just after a disturbance is indicated by t_1; t_2 relates to a short time after the disturbance; t_3 relates to the time when all short-term dynamics are in equilibrium. The load is assumed to have long-term constant power characteristics, but just after a disturbance, the load will initially change to a constant impedance characteristic. Then, by fast load restoration, the load is quickly restored to the pre-disturbance level.

The initial OC is found in point A'. Just after the disturbance, the short-term dynamics of system components such as generators or excitation systems will not yet have stabilized, which has the effect of shifting the post-disturbance $P - V$ curve to the left. As a result of the initial load characteristics and the shifted transient $P - V$ curve, the operating point moves along the arrow to operating point B'. After this transition, both the load and the post-disturbance $P - V$ curve are shifted towards their stable counterparts. However, due to the fast load dynamics, there exists no intersection between the load curve and the post-disturbance $P - V$ curve at t_2 (the area indicated with the red dotted circle), and without any emergency control actions, the system stability would be lost. Thus, even though the post-disturbance $P - V$ curve and the load characteristic at t_3 still intersect in this case, the system would have become unstable.

Instability caused by the short-term dynamics that follows a disturbance can generally be divided into three different instability mechanisms [1,3]:

- Loss of post-disturbance equilibrium of short-term dynamics: Typically exemplified by the stalling of induction motors after a disturbance causing the transmission impedance to increase. Due to the
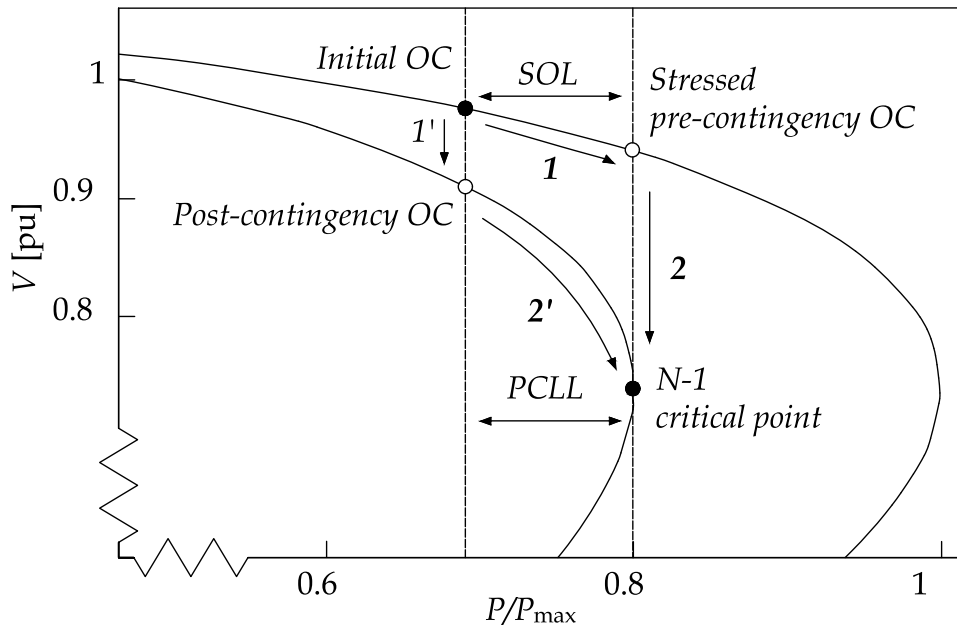

Fig. 1. Security margin estimation for PCLL and SOL. **1′** and **2′** illustrates the computation path for the PCLL; **1** and **2** illustrates the computation path for the SOL.
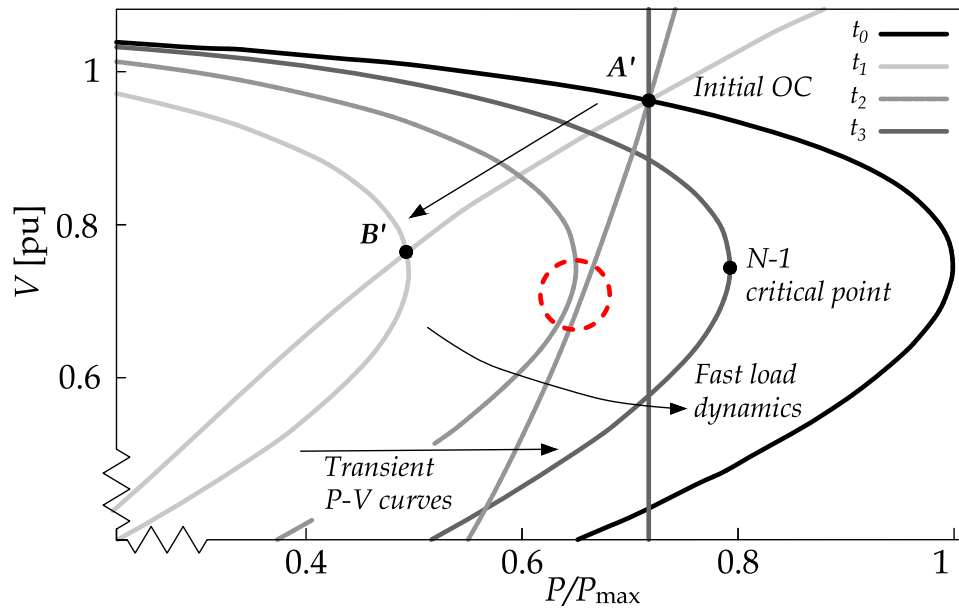
Fig. 2. Transient *P-V* curves illustrating a short-term instability event [16].

increased transmission impedance, the mechanical and electrical torque curves of the motor may not intersect, causing the system to lack a post-disturbance equilibrium, similar to the case illustrated in Fig. 2.

- Lack of attraction towards the stable post-disturbance equilibrium of short-term dynamics: Typically exemplified by transient angle instability and the loss of synchronism by one (or several) generators following a too slow fault clearing.
- Oscillatory instability of the post-disturbance equilibrium: Typically exemplified by rotor angle stability, in which the equilibrium between electromagnetic torque and mechanical torque of synchronous machines in the system is disturbed. Instability may be caused by increasing angular swings of some generators leading to their loss of synchronism with other generators [3].

Typically, time-domain simulations are required to capture the short-term dynamics after a large disturbance. SOLs computed using QSS simulations can not account for the short-term dynamics that follow after a disturbance and are thus better suited to only monitor long-term voltage instability phenomena. Extensions of the QSS model have been proposed that are capable of also incorporating frequency dynamics that take place over the same time scale as a long-term voltage instability event [11,21]. Combinations of time-domain simulations and QSS, as proposed in [11], can use time-domain simulations to model the system during the short-term period following a disturbance, followed by QSS simulations used to simulate the long-term interval after the short-term effects are finalized. However, short-term instability may also be induced by long-term dynamics, where the system degradation caused by long-term instability eventually can trigger the above-mentioned short-term events [1]. It should be noted that SOLs computed by combinations of time-domain simulations and QSS, as proposed in [11], cannot capture this type of event.

3. Methodology for security margin computations

In this section, the methodology used in the comparison between the PCLL and the SOL is presented. The load models and a description of the test system are presented along with the required adaptions. Finally, the methodology used to allow a fair comparison of the PCLL and the SOL is presented.

3.1. Load models

The power consumption of loads is generally affected by the system voltages and different load models are often used to characterize this relationship. A traditional load model used in both static and dynamic stability analysis is the ZIP model, which is made up of three components: constant impedance (Z), constant current (I), and constant power (P). The characteristics of the ZIP model is given by [1]:

$$P = zP_0 \left[a_P \left(\frac{V}{V_0} \right)^2 + b_P \frac{V}{V_0} + c_P \right] \tag{1a}$$

$$Q = zQ_0 \left[a_Q \left(\frac{V}{V_0} \right)^2 + b_Q \frac{V}{V_0} + c_Q \right] \tag{1b}$$

where $a_P + b_P + c_P = a_Q + b_Q + c_Q = 1$, P_0 and Q_0 are the real and reactive powers consumed at a reference voltage V_0, given that $z = 1$. V is the actual voltage and z is a variable indicating the actual loading of the system [1]. The constants a_x, b_x, and c_x represent the share of constant impedance, constant current, and constant power of the load, respectively.

Although simple and widely used in security analysis [22], the ZIP model cannot model any dynamic behavior of the loads themselves. The significance of induction motor loads and other fast-acting dynamic loads are often highlighted in system stability studies. Induction motors (IM) are characterized by fast load restoration dynamics (often in the time frame of a second) and have a high reactive power demand. Induction motors are also prone to stalling, which may cause the motor to draw high reactive currents from the grid, resulting in a deteriorating effect on the system stability [1]. In PSS®E, a complex load model (CLOD) can be used to represent a bundled mix of loads with different dynamic load characteristics into a single model. The CLOD models a composition of various load types including induction motors and several static loads but requires only eight parameters, which is achieved by internally using typical manufacturer data for each load type. The CLOD model was chosen as it provides a simple yet efficient solution to model different configurations of common load types, including induction motors, when no detailed dynamics data were available. In Fig. 3, a schematic of the CLOD model is presented. The transformer and feeders connecting the system bus to the load bus are modeled as a single impedance. At the load bus, different percentages of large and small IMs,
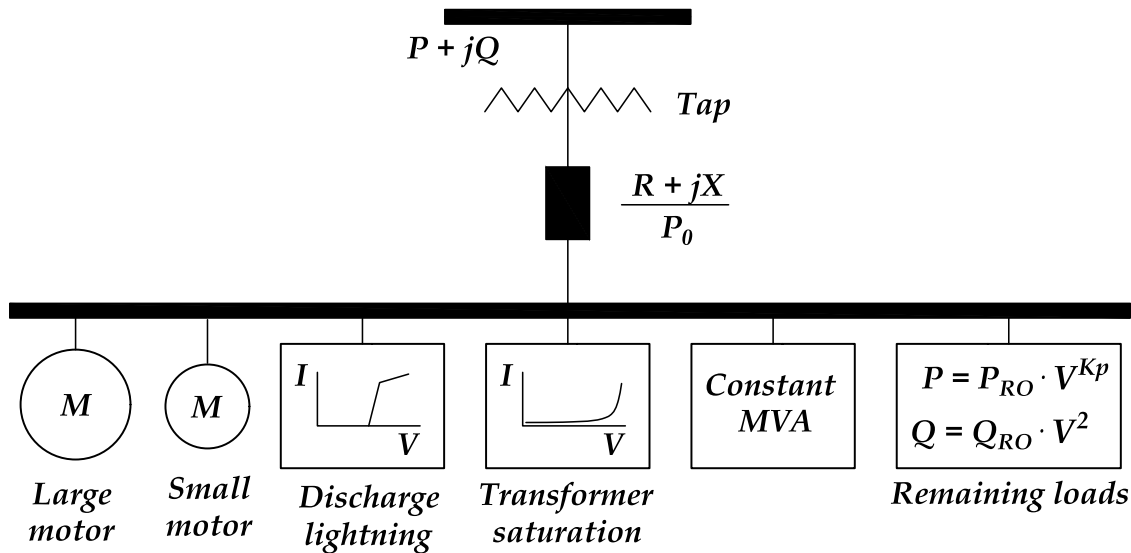
Fig. 3. Overview of the complex load model (CLOD) [23].

discharge lighting loads, transformer saturation, and constant power loads can be modeled. The remaining part of the load is modeled as a polynomial load where the voltage dependency of the active load is controlled through a constant K_p. The performance curves of the two motor models, the discharge lightning model, and the transformer saturation model is further detailed in [23].

It should be noted that all constant power loads in PSS®E are modeled as constant power only for a certain range of load voltages. When voltages drop below a threshold, by default 0.7 per unit in PSS®E, the constant power loads instead follow a function based on the magnitude of the bus voltage, further detailed in [24].

3.2. Simulation test system

All simulations have been tested on the slightly modified version of the Nordic32 test system, detailed in [25]. The main characteristic of the system is sensitivity towards long-term voltage instability, although the system can exhibit other types of instabilities as well. A single-line diagram of the test system is presented in Fig. 4. The security margins are computed by increasing the loading in the area "*Central*", while the generation in the area "*North*" is increased by a corresponding quantity. The starting point for all scenarios is the secure "operating point B" as defined in [25].

All simulations were carried out using PSS®E version 35.0. To ensure numerical stability during the dynamical simulation runs, a short integration step of 0.001 s was used in the simulations. In certain sensitive scenarios, such as when the simulations resulted in a non-converging dynamic simulation, the integration step was at times varied to provide a converging simulation.

3.3. Methodology and adaptations

To compare the two conceptually different methods of PCLL and SOL is not trivial; one is computed using a static model of the system, while the other is generally estimated using a dynamic model. To ensure that the difference in the computed security margins was not caused by differences in how the simulations were conducted, but rather by the fact that the SOL could better account for the system's dynamic response after a disturbance, a few adaptations of the methods were required. Instead of using CPF methods to compute the PCLL, we adopted a method that *slowly* ramps up the system stress in a dynamic simulation setting; an approach similar to the one used to compute the (pre-contingency) loadability margins in [25]. This approach allows the PCLL to

be performed in a dynamic setting while mimicking how the system stress would have been increased if it would have been performed in a static setting. The advantage of adopting this methodology is that the loading and the generation set points could be increased in the *exact* same way for both the computation of the PCLL and the SOL.

In [25], when computing the PCLL, the authors increased the system stress in small increments over time but did not evaluate whether the system had stabilized before continuing stressing the system. This could result in that additional system stress was added to an already unstable system and that the PCLL became overestimated. For instance, long-term voltage instability events typically last several minutes, and a significant amount of system stress could thus have been added to the system while it had already become unstable. To address this issue, we used an adaptive method to analyze whether the system had stabilized. To achieve this, the timer settings of LTCs and over-excitation limiters (OELs) were monitored continuously throughout the simulation. The LTC timers are activated whenever the voltage at a controlled bus is below (or above) a certain controlled bound. The OEL timers are activated whenever the field current of a generator is above a certain threshold. The specific timer settings for the OELs is computed by a function based on the magnitude of which the threshold is exceeded, see [26]. If the controlled voltages, respectively the field currents, are restored within the controlled bounds, respectively the field current thresholds, the timers are reset. These two components have the longest timer settings in the test system, and if all timers were reset for a given time (3 s) after a disturbance (or a load increase), the system was assumed to have stabilized.

3.3.1. Steps for PCLL computation

The steps used in computing the PCLL were the following:

- **Initialization:** The PCLL computation was initialized by applying a chosen contingency in the system in a dynamic simulation from the base case. The dynamic simulation ran until the system was fully stabilized.
- **Increase system stress:** Once the system had stabilized after the initial disturbance, the system stress was increased in small increments of 1 MW, which was distributed among all the loads in the "*Central*" area. To reduce the required simulation time, the system stress was for certain fault scenarios (scenarios A and B) initially increased in larger increments (5 MW), since lower stress levels were found to not cause instability in the system. The different fault scenarios are further discussed in Section 4.1. The power factor of each
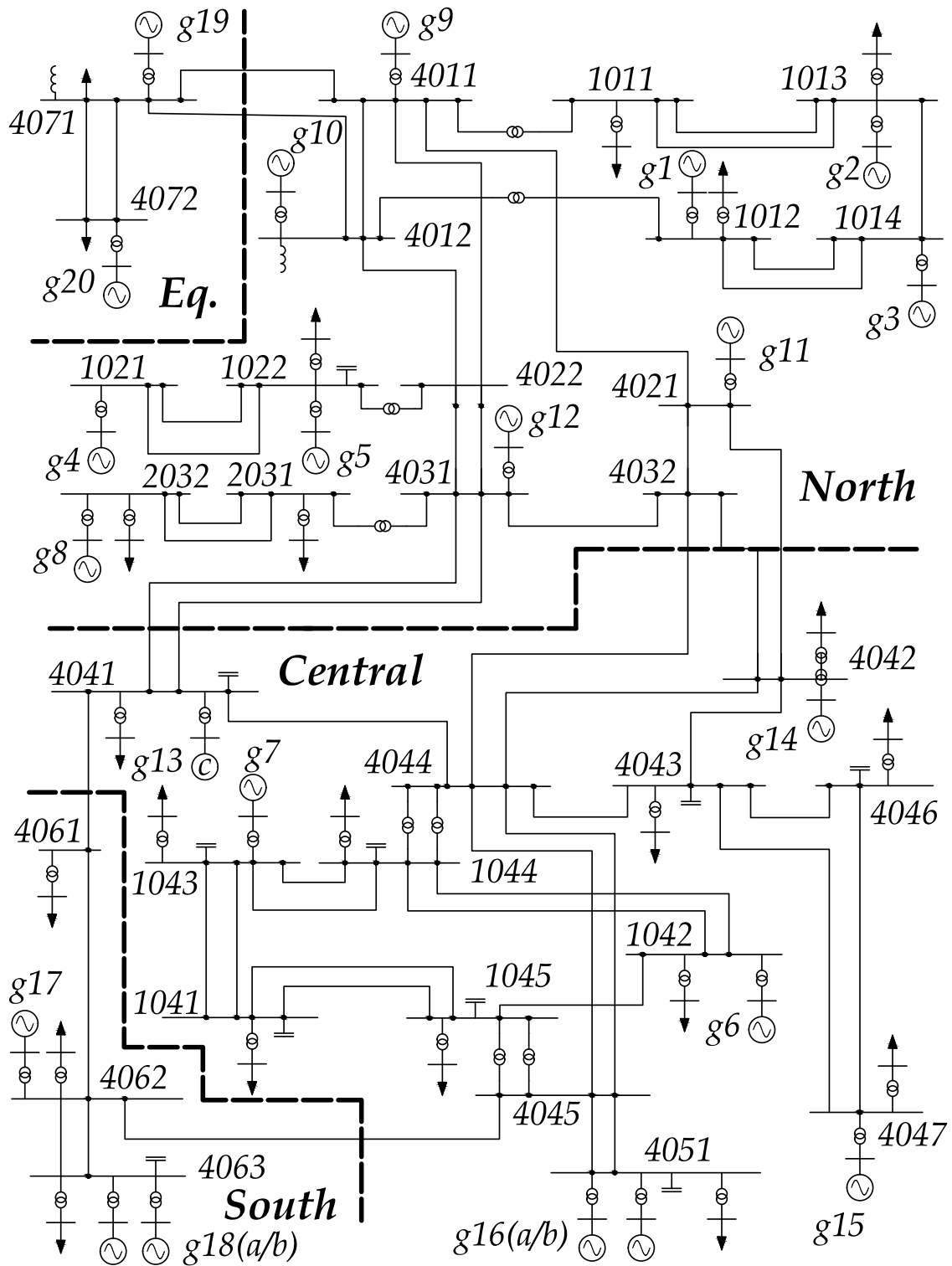
Fig. 4. Single-line diagram of the modified Nordic32 system [25].

load was kept constant. Simultaneously, the load change was compensated by the primary frequency response of the generators in the system. The added load for both the PCLL and SOL were computed as a nominal load increase at 1.0 pu voltage to ensure that the same amount of load was added for both methods regardless of the current load voltage in the dynamic simulation. Increased active line losses caused by the increased system stress were also automatically compensated by the generators' primary frequency

response, while the reactive line losses were automatically compensated by the generators' excitation systems.

- **Check stability criterion:** After the increased system stress, the simulation continued to run until the system either stabilized or until the stability criterion was violated. The system was considered unstable if *any* bus voltage in the system was lower than 0.9 pu. Although the modified Nordic32 test system is characterized by sensitivity towards voltage instability, other types of instability can violate the stability criterion. For instance, transient angle instability

can cause locally low voltages due to lost synchronism of certain generators. Overloading of transmission lines and transformers was not included in the stability criteria, as it is not directly affected by the dynamics of the system, but mainly just the magnitude of the system stress. Thus, in those cases that overloading would affect the results and be limiting for the security margin, it would generally limit the PCLL and the SOL to the same degree.

- **Re-iterate:** The system stress was increased until the system eventually violates the stability criterion. The difference in loading from the base case to the final stable operating point in the stressed post-contingency system represents the computed PCLL.

3.3.2. Steps for SOL computation

The SOL was computed similarly to the PCLL, but by instead stressing the system in its pre-contingency configuration and *then* introducing the disturbance. The steps used in the computation of the SOLs were the following:

- **Initialize simulation and increase system stress:** When the ZIP model was used to model the loads, the dynamic simulation was initialized directly at the beginning of the simulation. The system stress was then increased in its *pre-contingency* base case in small increments of 1 MW, in the same way as was done for the PCLL computation in its post-contingency configuration. The small step size in system stress was chosen to allow the illustration of the security margins using *P-V* curves. In more general applications, faster methods such as the binary search method described in [10] or the dual binary search method described in[16], can otherwise be used to compute the SOL.

  Adjustments for the CLOD model: For the scenarios using the CLOD model, the increased system stress was required to be added in a static load flow scenario, which was then converted for dynamical studies. The increased load was distributed in a similar manner as when using the ZIP load model, except that the load was added in a static load flow scenario instead of during a dynamic simulation. However, the increased load could now not be automatically compensated by the generators' primary frequency response, and the increased load was instead distributed and compensated by increasing the generation set-points of all the hydro generators in the "North" and "Eq" regions, see Fig. 4. The distribution of the increased generation was based on the rated capacity of each generator and a generator with a higher rated capacity received a larger share of the increased generation. Increased active line losses caused by the increased system stress were compensated by an increase in the generation of the slack bus generator, "g20". While this distribution can be assumed to be relatively similar to how the primary frequency control of the governors would have compensated for the increased load, it will cause a small difference in how the system stress is increased between the two load models.

- **Introduce disturbance and check stability:** A disturbance was then applied in the system. A final end time of the dynamic simulation of 1000 s was used. The system was considered unstable if *any* bus voltage in the system was lower than 0.9 pu at the end of the simulation. The simulation was also stopped in advance if any bus voltage decreased below 0.7 pu (still allowing the system to first stabilize for 20 s after the disturbance).

- **Re-iterate:** If the system was stable, the system was reinitialized to the last pre-contingency state, followed by increasing the system stress by an additional 1 MW and applying the same disturbance. The SOL is then computed from the difference in loading from the base case to the final stable operating point in the stressed post-contingency system.

4. Simulation results and discussion

In this section, the results of the numerical comparison between the PCLL and the SOL are presented. Three different contingency scenarios were tested. The results of PCLL and the SOL computation are presented for each contingency scenario and each load model configuration. It should be noted that the different types of disturbances were chosen to exemplify the difference between the two security margin methods under various conditions. In real applications, all relevant contingencies that might be dimensioning for the security margin should be analyzed. In general, system operators perform contingency filtering (or selection) as it would be computationally infeasible to analyze *all* possible disturbances that might occur [10]. Furthermore, the direction of the system stress and the load-generation configuration should be representative of the specific system in consideration.

4.1. Contingency scenarios and loading scenarios

The following contingency scenarios were examined:

- **Scenario A:** A three-phased fault for 40 milliseconds, followed by tripping the faulted line. The faulted line is the one connecting the two areas "*North*" and "*Central*" between bus 4032 to bus 4044.
- **Scenario B:** A longer three-phased fault for 100 milliseconds, followed by tripping the faulted line. The faulted line is the one connecting the two areas "*North*" and "*Central*" between bus 4032 to bus 4044.
- **Scenario C:** Tripping of generator "g7" located at bus 1043 in the "*Central*" area.

For each of the contingency scenarios, different combinations of the ZIP load were tested for both the PCLL and the SOL. In addition, the SOL was computed for different compositions when the CLOD model was used to model the loads in the system. Adjusting the load levels *during* a dynamic simulation, which was required when computing the PCLL, was not feasible when using the CLOD model, as it requires that its internal parameters are recomputed whenever the load composition changes. Thus, the CLOD model was analyzed only with respect to the SOL. Furthermore, the CLOD model was found to be generally numerically unstable for longer fault clearing times. Thus, we only provide a comparison of the results for Scenario A with a fault clearing time of 40 milliseconds.

4.2. Simulation results

The PCLL and SOL results for each scenario and each load configuration using the ZIP model are presented in Table 1. The SOL results for scenario A and different configurations of the CLOD model are presented in Table 2. The largest difference between the PCLL and SOL is found for cases with a high share of constant power characteristics of the active part of the loads. For instance, for scenario 1A with fully constant power characteristics for the active part of the load and fully constant impedance characteristics for the reactive part of the load, the SOL was only 28 MW, while the PCLL was found to be 275 MW. The difference between the two security margin methods then reduces rapidly with a decreasing level of constant power characteristics on the active part of the load. Already at slightly lower levels of constant power loads, for instance, in Scenario 4A, the difference between the SOL and the PCLL becomes close to negligible. In Fig. 5, the post-disturbance *P-V* curves of the transmission side of bus 1041 are illustrated, respectively, for Scenario 1A. The *P-V* curves are computed by sampling the voltage magnitude when the system had stabilized after each dynamic simulation. Here, with a fully constant power characteristic of the active part of the loads, the *P-V* curves are almost identical for both the PCLL and the SOL up until the collapse point for the SOL.

The difference between the PCLL and the SOL is more significant for Scenario B when a longer fault clearing time was used in the simulations. For instance, in Scenario 1B, the SOL was estimated to only 4 MW, compared to 275 MW for the PCLL. With reference to the discussion with

Table 1
Computed PCLL and SOL for different loading and contingency scenarios.

	Constant			Scenario A		Scenario B		Scenario C	
	MVA	I	Z						
Scenario number	(P/Q) [%]	(P/Q) [%]	(P/Q) [%]	PCLL [MW]	SOL [MW]	PCLL [MW]	SOL [MW]	PCLL [MW]	SOL [MW]
1	100/0	0/0	0/100	275	28	275	4	351	71
2	95/0	5/0	0/100	340	88	340	86	353	128
3	90/0	10/0	0/100	341	146	341	144	357	196
4	80/0	20/0	0/100	364	362	364	260	365	362
5	50/0	50/0	0/100	387	386	387	387	380	378
6	95/0	5/50	0/50	280	55	280	48	283	85
7	80/0	20/50	0/50	359	240	359	233	357	356
8	50/0	50/50	0/50	382	382	382	381	375	372
9	0/0	100/0	0/100	425	424	425	425	407	405
10	0/0	50/0	50/100	465	464	465	456	439	438
11	0/0	20/0	80/100	488	488	488	489	457	458
12	0/0	0/0	100/100	504	504	504	505	471	471

Table 2
SOLs for different load configurations of the CLOD model.

	CLOD model parameters						Scenario A
Scenario number	LIM [%]	SIM [%]	DL [%]	TS [%]	MVA [%]	Remaining ($K_p = 2$) [%]	SOL [MW]
13	35	35	5	5	10	10	-
14	30	30	5	5	10	20	60
15	25	25	5	5	10	30	372
16	35	30	5	5	10	15	28
17	35	25	5	5	10	20	47
18	35	20	5	5	10	25	59
19	30	35	5	5	10	15	37
20	25	35	5	5	10	20	120
21	20	35	5	5	10	25	365

the transient *P-V* curves presented in Section 2.2, a longer fault clearing time would have the effect of shifting the post-disturbance $P - V$ curve for a longer time to the left, causing the system to lack attraction towards a stable post-disturbance equilibrium. Yet again, the difference between the two security margins decreases rapidly as the share of constant active power loads decreases. For instance, in Scenario 5B with a 50% share constant active power load, and the remaining part of the active load being of constant current characteristics, the SOL and the PCLL are almost identical. The post-disturbance *P-V* curves of scenario 5B on the transmission side of bus 1041 are illustrated in Fig. 6. The figure shows that although the computed *P-V* curves of the SOL are slightly below that of the PCLL, the two security margins find almost the same critical point of the system.

For all cases, except when the load is of constant power characteristics, the *P-V* curves computed using the SOL are *slightly* below the ones computed using the PCLL. Although the initial response of the excitation systems used in the Nordic32 test system is fast, there is an integrating part of the control system which takes a longer time until the voltage
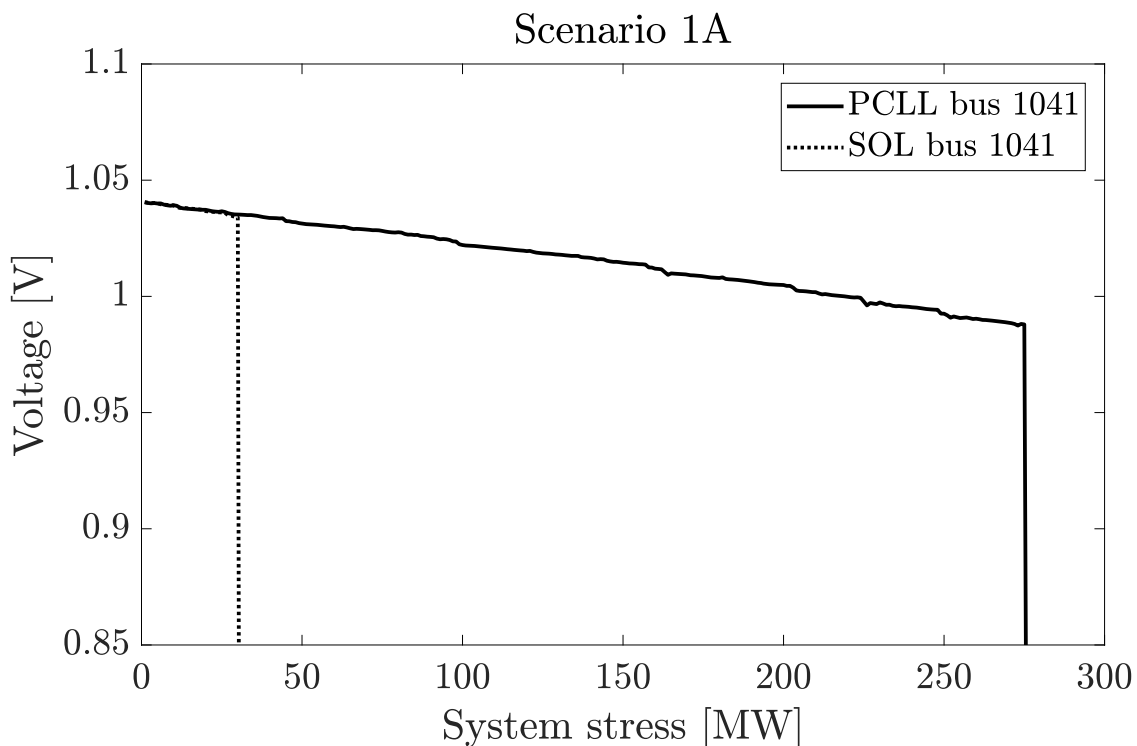
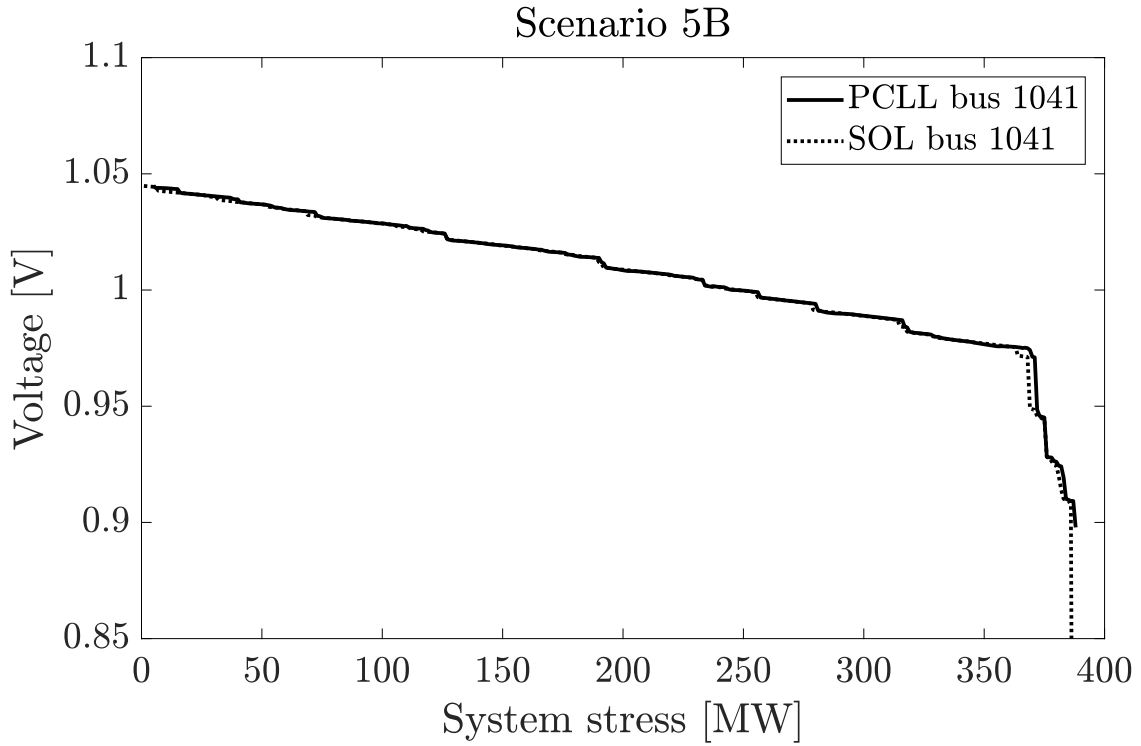**Fig. 5.** *P-V* curves computed at bus 1041 for scenario 1A.

Fig. 6. *P-V* curves computed at bus 1041 for scenario 5B.

magnitudes of the generators are restored to their pre-disturbance set-point (differing slightly due to the droop in the automatic voltage regulation). In the PCLL case, this voltage restoration is allowed to fully stabilize after the initial disturbance before the system stress is added to the system. This is not the case for the SOL, in which the system is stressed before the disturbance is applied to the system. In turn, this causes LTCs and OELs to act earlier for a lower level of system stress, causing the magnitude of the post-disturbance voltages to be generally lower.

In Scenario C, the chosen contingency was the disconnection of the generator "g7", located in the "*Central*" area. Once again, the largest difference between the PCLL and SOL is found for cases with a high share of constant power characteristics of the active part of the loads. For load scenarios with a larger share of either constant current or constant impedance characteristics of the active part of the load, the difference between the two security margins becomes negligible.

In Table 2, the computed SOLs for scenario A when using different configurations of the CLOD model are presented. The scenarios are generated by varying the load composition, consisting of large induction motors (LIMs), small induction motors (SIMs), discharge lightning (DL), transformer saturation (TS), constant power loads (MVA), and the remaining load which is of constant impedance characteristics ($K_p = 2$). Unsurprisingly, the computed SOL was the lowest when there was a large share of motor loads in the system. When the loads were modeled with a *too* high share of motor loads, such as scenario 13A, the computed SOL for the base case was negative. There was a relatively large difference between the computed SOL for scenario 17A with a 35% share of LIM loads and 25% share SIM loads, and scenario 20A with a 25% share of LIM loads and 35% share of SIM loads. LIM loads generally draw a higher reactive current during instances of low system voltages than SIM loads, which may have caused the computed SOL to differ from 47 MW for scenario 17A to 120 MW for scenario 20A.

In most scenarios where the CLOD model was used and for the level of system stress that made the system unstable, the system crashed during the transient state just after the disturbance. The CLOD models were found to be particularly sensitive towards long fault clearing times,

and the Nordic32 test system consistently crashed when using a longer fault clearing time (such as 0.1 s). The difference between the two security margins is thus likely even greater if breakers with longer fault clearing times can be assumed to dominate the system. However, in a few scenarios, the long-term load restoration in the system was the main driver for instability. One of these cases, scenario 15A, is illustrated in Fig 7, which shows the development of bus voltages over time for different levels of system stress. For the lower system stress levels of 150 MW and 372 MW, the system is able to satisfy the given stability criterion, although the 372 MW level causes the system voltages to drop significantly. However, for a system stress level of 373 MW, the long-term load restoration and the activation of OELs cause the system to lose stability after about 500 s.

4.3. Discussion

The results in the previous section show that although the *same* operating point has been used as a starting point for all scenarios, the PCLL and the SOL differ significantly depending on the current load configuration and the type of fault that is considered. The largest difference between the two security margin methods was found when either the loads were of high constant power characteristics or consisted of a large penetration of induction motor loads. These results thus confirm the well-known fact that loads with fast restoration dynamics (where a constant power characteristic can be considered a theoretic extreme case) will deteriorate the system stability, and illustrate how significant this impact may be on the computed security margins.

The main conclusions of this study, that high penetration of loads with fast restoration dynamics will result in a difference between the PCLL and the SOL, should generalize well to other types of power systems. However, care should be taken when generalizing the *specific* results of this study to real power systems with different characteristics. For instance, although the difference between the SOL and the PCLL in this study was found to be negligible whenever the share of constant power characteristic of the active part of the loads was lower than 50%, this is not necessarily the case for other systems with different dynamics.
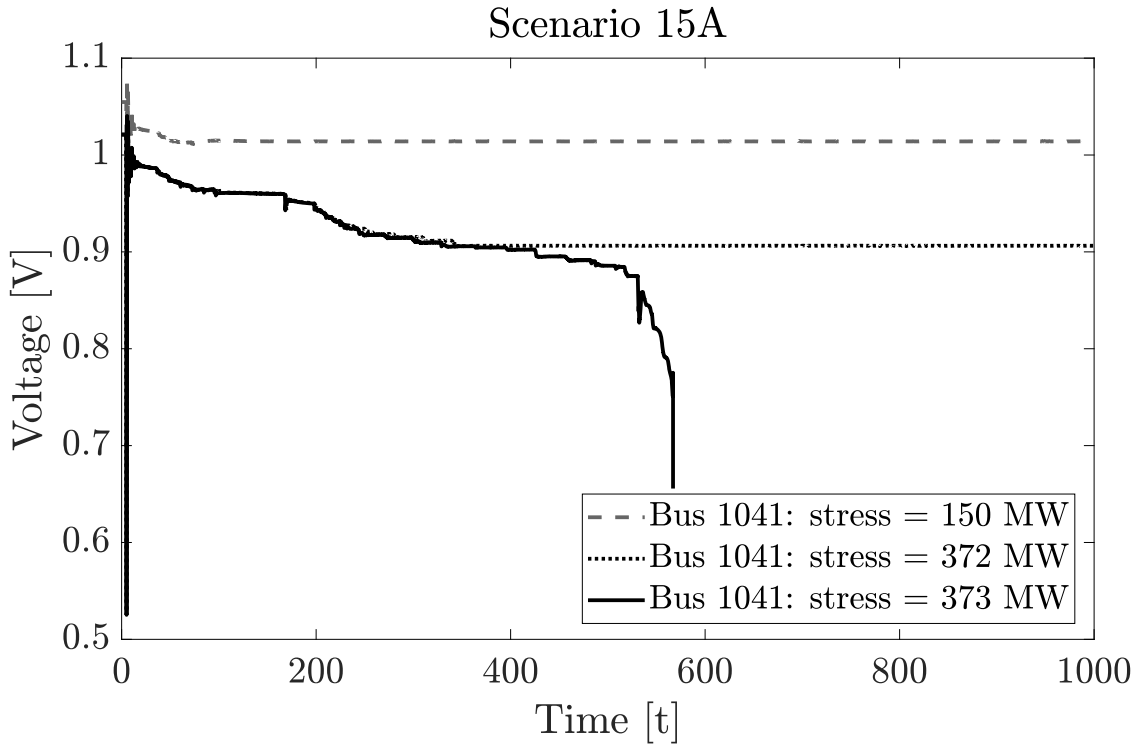
Scenario 15A

Fig. 7. Voltage evolution for bus 1041 for Scenario 15A for different levels of system stress.

System operators would thus be required to perform a similar analysis on their specific systems to analyze during what specific loading scenarios the PCLL and the SOL start to differ.

The stability assessment practice of many system operators is, to the authors' best knowledge, to compute security margin estimations computed by PCLLs, often in combination with dynamic security assessment (DSA). While DSA can provide certain types of security margins based on indices such as the transient energy functions [27], it does not provide an accurate measure of the loadability limit to the point where the system can no longer remain secure. We believe that if system operators continue to rely on conventional security margins computed by the PCLL, it is important to verify the reliability of those security margins to avoid either overly optimistic security margins or to avoid having to add unnecessary large reliability margins to the computed security margins. To account for modeling inaccuracies, transmission reliability margins are often added to ensure that modeling inaccuracies will not cause the system to be operated unknowingly in a non-secure operating state. Thus, if more accurate methods to determine security margins are used, such as the SOL, these reliability margins may theoretically be reduced and the system operators could more efficiently utilize the existing transmission capacity.

Dynamic load modeling may also become increasingly important in the future, as more loads are expected to be controlled through power electronically-controlled interfaces. These types of loads, such as electric vehicle chargers, inhibit very fast dynamic responses after disturbances [28]. Despite this, dynamic load models are still relatively unused in the industry. In a large survey study from 2013 on international industry practice on power system load modeling, it was shown that about 70% of system operators and utilities still only used static load models for power system stability studies [29]. A drawback of advanced load models is that the load composition is often partly unknown to system operators, and it is thus more straightforward to use the simplified static load models. Another drawback is the increase in computational requirement during simulations, which reduces their applicability in real-time applications. However, although complex load models do not necessarily need to be used in real-time applications, sensitivity analyses can

preferably be performed using these models, so that the impact of various degrees of motor loads and other types of loads on the stability of a system can be studied.

While this study focused on the impact of different load models, converter-interfaced generation and other power electronic devices in the power system will also have a significant impact on the computed security margins. Although a growing share of renewable generation is often challenging from a planning perspective due to the intermittency of the energy source, the converter interface may in fact mitigate some of the short-term instability phenomena. For instance, with proper design of the converter controls, such components can contribute in providing fast voltage/reactive power control or active power control for fast frequency responses. We argue that the impact of such components, also in combination with loads with fast restoration dynamics, deserves further attention in future research.

5. Conclusions

In this paper, the PCLL and the SOL have been compared and studied under various load configurations and disturbance scenarios. A methodology was developed to allow a fair comparison between the two methods to ensure that the difference in the computed security margins was due to actual differences of the security margin approaches, and not caused by differences in the simulation setups. The numerical comparison shows that the two methods differ significantly under various load configurations and fault scenarios. The largest difference between the two methods was found when the loads were of high constant power characteristics or when the loads consisted of a large share of induction motor loads. Furthermore, the fault clearing time is found to be especially important and a longer fault clearing time caused the SOL to become significantly smaller than the PCLL. The results highlight the importance of load modeling and show that if a power system can be expected to have a large share of loads with fast restoration dynamics, the conventional method of using PCLL to compute the security margins can provide overly optimistic values of the actual security margin.

CRediT authorship contribution statement

Hannes Hagmar: Conceptualization, Methodology, Software, Writing – original draft. **Le Anh Tuan:** Writing – review & editing, Supervision, Project administration, Funding acquisition. **Robert Eriksson:** Writing – review & editing, Supervision, Project administration.

Declaration of Competing Interest

The authors declare that they have no known competing financial interests or personal relationships that could have appeared to influence the work reported in this paper.

References

[1] T. Van Cutsem, C. Vournas, Voltage Stability of Electric Power Systems, Kluwer Academic Publishers, Boston, 1998.

[2] C. Vournas, T. Van Cutsem, Online voltage security assessment. Real-Time Stability in Power Systems, Springer, 2014, pp. 305–333.

[3] N. Hatziargyriou, J.V. Milanovic, C. Rahmann, V. Ajjarapu, C. Canizares, I. Erlich, D. Hill, I. Hiskens, I. Kamwa, B. Pal, P. Pourbeik, J.J. Sanchez-Gasca, A. M. Stankovic, T. Van Cutsem, V. Vittal, C. Vournas, Definition and classification of power system stability revisited & extended, IEEE Trans. Power Syst. (2020), https://doi.org/10.1109/TPWRS.2020.3041774.Early access

[4] A. Adrees, J. Milanović, Effect of load models on angular and frequency stability of low inertia power networks, IET Gener. Transm. Distrib. 13 (9) (2019) 1520–1526.

[5] T. Souxes, C. Vournas, System stability issues involving distributed sources under adverse network conditions. Proc. IREP Symp. Bulk Power System Dyn. Control-X (IREP), 2017, pp. 1–9.

[6] B. Kroposki, B. Johnson, Y. Zhang, V. Gevorgian, P. Denholm, B. Hodge, B. Hannegan, Achieving a 100% renewable grid: Operating electric power systems with extremely high levels of variable renewable energy, IEEE Power Energy Mag. 15 (2) (2017) 61–73, https://doi.org/10.1109/MPE.2016.2637122.

[7] R.F. Mochamad, R. Preece, Assessing the impact of VSC-HVDC on the interdependence of power system dynamic performance in uncertain mixed AC/DC systems, IEEE Trans. Power Syst. 35 (1) (2020) 63–74, https://doi.org/10.1109/TPWRS.2019.2914318.

[8] S.F. Santos, M. Gough, D.Z. Fitiwi, A.F.P. Silva, M. Shafie-Khah, J.P.S. Catalão, Influence of battery energy storage systems on transmission grid operation with a significant share of variable renewable energy sources, IEEE Syst. J. (2021) 1–12, https://doi.org/10.1109/JSYST.2021.3055118.

[9] U. Datta, A. Kalam, J. Shi, Battery energy storage system to stabilize transient voltage and frequency and enhance power export capability, IEEE Trans. Power Syst. 34 (3) (2019) 1845–1857, https://doi.org/10.1109/TPWRS.2018.2879608.

[10] T. Van Cutsem, C. Moisse, R. Mailhot, Determination of secure operating limits with respect to voltage collapse, IEEE Trans. Power Syst. 14 (1) (1999) 327–335, https://doi.org/10.1109/59.744551.

[11] T. Van Cutsem, M.-E. Grenier, D. Lefebvre, Combined detailed and quasi steady-state time simulations for large-disturbance analysis, Int. J. Electr. Power Energy Syst. 28 (9) (2006) 634–642, https://doi.org/10.1016/j.ijepes.2006.03.005.

[12] A. Kaci, I. Kamwa, L.-A. Dessaint, S. Guillon, Synchrophasor data baselining and mining for online monitoring of dynamic security limits, IEEE Trans. Power Syst. 29 (6) (2014) 2681–2695.

[13] A. Sittithumwat, K. Tomsovic, Dynamic security margin estimation using artificial neural networks. IEEE Power Engineering Society Summer Meeting, Chicago, IL vol. 3, 2002, pp. 1322–1327, https://doi.org/10.1109/PESS.2002.1043583.

[14] N. Amjady, Dynamic voltage security assessment by a neural network based method, Electr. Power Syst. Res. 66 (3) (2003) 215–226, https://doi.org/10.1016/S0378-7796(03)00048-8.

[15] M.V. Baghmisheh, H. Razmi, Dynamic voltage stability assessment of power transmission systems using neural networks, Energy Convers. Manage. 49 (1) (2007) 1–7, https://doi.org/10.1016/j.enconman.2007.06.017.

[16] H. Hagmar, R. Eriksson, A.T. Le, Fast dynamic voltage security margin estimation: concept and development, IET Smart Grid 3 (4) (2020), https://doi.org/10.1049/iet-stg.2019.0278.

[17] I. Dobson, The irrelevance of load dynamics for the loading margin to voltage collapse and its sensitivities. Bulk Power System Voltage Phenomena - III: Voltage Stability, Security & Control, 1994, pp. 509–518.

[18] B.H. Chowdhury, C.W. Taylor, Voltage stability analysis: V-Q power flow simulation versus dynamic simulation, IEEE Trans. Power Syst. 15 (4) (2000) 1354–1359, https://doi.org/10.1109/59.898112.

[19] V. Ajjarapu, C. Christy, The continuation power flow: a tool for steady state voltage stability analysis, IEEE Trans. Power Syst. 7 (1) (1992) 416–423, https://doi.org/10.1109/59.141737.

[20] M.K. Pal, Voltage stability conditions considering load characteristics, IEEE Trans. Power Syst. 7 (1) (1992) 243–249, https://doi.org/10.1109/59.141710.

[21] M.-E. Grenier, D. Lefebvre, T. Van Cutsem, Quasi steady-state models for long-term voltage and frequency dynamics simulation. 2005 IEEE Russia Power Tech, 2005, pp. 1–8, https://doi.org/10.1109/PTC.2005.4524400.

[22] A. Arif, Z. Wang, J. Wang, B. Mather, H. Bashualdo, D. Zhao, Load modeling-a review, IEEE Trans. Smart Grid 9 (6) (2018) 5986–5999.

[23] PSS®E 35.0.0 Program Application Guide: Volume II, Siemens Power Technologies International, Schenectady, NY, 2019a.

[24] PSS®E 35.0.0 Program Application Guide: Volume I, Siemens Power Technologies International, Schenectady, NY, 2019b.

[25] T. Van Cutsem, M. Glavic, W. Rosehart, C. Canizares, M. Kanatas, L. Lima, F. Milano, L. Papangelis, R.A. Ramos, J.Ad. Santos, B. Tamimi, G. Taranto, C. Vournas, Test systems for voltage stability studies, IEEE Trans. Power Syst. 35 (5) (2020) 4078–4087.

[26] PSS®E 35.0.0 Model Library, Siemens Power Technologies International, Schenectady, NY, 2019.

[27] J.L. Jardim, Online dynamic security assessment. Real-Time Stability in Power Systems, Springer, 2014, pp. 159–197.

[28] D. Mao, K. Potty, J. Wang, The impact of power-electronics-load dynamics on large-disturbance voltage stability. 2018 IEEE Power Energy Society General Meeting (PESGM), 2018, pp. 1–5.

[29] J.V. Milanovic, K. Yamashita, S. Martínez Villanueva, S.Z. Djokic, L.M. Korunović, International industry practice on power system load modeling, IEEE Trans. Power Syst. 28 (3) (2013) 3038–3046.